Title page

Title

Salience network atrophy links neuron type-specific degeneration to loss of empathy in frontotemporal dementia

Authors

Lorenzo Pasquini[1], Alissa L. Nana[1], Gianina Toller[1], Jesse Brown, [1]Jersey Deng[1], Adam Staffaroni[1], Eun-Joo Kim[1], Ji-Hye L. Hwang[1], Libo Li[1,3], Youngsoon Park[1], Stephanie E. Gaus[1], Isabel Allen[1], Virginia E. Sturm[1], Salvatore Spina[1], Lea T. Grinberg[1], Katherine P. Rankin[1], Joel Kramer[1], Howard H. Rosen[1], Bruce L. Miller[1], William W. Seeley[1,2]

Affiliations

Department of Neurology[1] and Pathology[2], Memory and Aging Center, University of California San Francisco, San Francisco, California USA, Department of Psychopharmacology, Qiqihar Medical University, Qiqihar, China[3]

Corresponding author:

William W. Seeley, MD. 675 Nelson Rising Lane 94158, San Francisco, California USA. Email: bill.seeley@ucsf.edu. Phone: +1-415-476-2793

Abbreviations

ALS = amyotrophic lateral sclerosis; bv = behavioral variant; *C9orf72* = chromosome 9 open reading frame 72; FI = frontoinsular cortex; FTD = frontotemporal dementia; MND = motor neuron disease; MRI = magnetic resonance imaging; TDP-43 = transactive response DNA binding protein 43 kD; VENs = von Economo neurons

Abstract

Each neurodegenerative syndrome presents with characteristic symptoms that reflect the specific pattern of cellular, regional, and large-scale network vulnerability. In behavioral variant frontotemporal dementia (bvFTD), a disorder of social-emotional function, von Economo neurons (VENs) and fork cells are among the initial cellular targets. These large layer 5 projection neurons are concentrated in the anterior cingulate and frontoinsular (FI) cortices, regions that anchor the salience network, a large-scale system linked to social-emotional function via roles in autonomic processing and homeostatic behavioral guidance. Here, we combined questionnaire-based empathy assessments, in vivo structural neuroimaging, and quantitative histopathological data from 16 patients across the FTD-amyotrophic lateral sclerosis clinicopathological spectrum linked to TAR DNA-binding protein 43 pathobiology. We sought to examine how neuron type-specific degeneration is linked to regional gray and white matter atrophy and, in turn, to loss of emotional empathy. We show that disease protein aggregation within right FI VENs and fork cells is associated with atrophy in insular, medial frontal, and subcortical regions including the dorsomedial thalamus that represent key nodes within the salience network. Gray and white matter degeneration within these structures, in turn, mediated loss of emotional empathy, suggesting a chain of influence linking the cellular, regional/network, and behavioral levels in producing the signature bvFTD clinical features. Overall, the findings suggest that VENs and fork cells facilitate specialized human social-emotional capacities by contributing to salience network function.

Keywords

Empathy, fork cells, frontoinsular cortex, frontotemporal dementia, salience network, von Economo neurons

Introduction

Growing evidence suggests that misfolded neurodegenerative disease proteins accumulate within vulnerable onset regions, presumably within the most vulnerable neurons therein, before spreading to other brain areas along large-scale brain network connections [1–3]. Although the mechanisms underlying cell type-specific vulnerability remain largely unknown, histopathological studies have identified distinct, topographically restricted neuronal populations targeted in each neurodegenerative syndrome [1,4]. For example, postmortem studies in Alzheimer's disease, the most common cause of dementia worldwide, show early tau deposition in neurons within the locus coeruleus, dorsal raphe nucleus, and the entorhinal cortex [5–7]. Postmortem histopathological [5] and in vivo neuroimaging [8] studies provide converging evidence that the disease progresses anatomically from these sites to brain areas functionally and structurally connected to the putative onset regions [9]. Similarly, studies in behavioral variant frontotemporal dementia (bvFTD) have revealed that von Economo neurons (VENs) and fork cells are the initial targets of the disease [10–12]. These neuronal morphotypes make up a unique class of large, bipolar layer 5 projection neurons, which, in large-brained highly social mammals, are concentrated in the anterior cingulate and anterior agranular insular (i.e. frontoinsular [FI]) cortices [13–15]. The anterior cingulate cortex and FI are known for their functional coactivation as part of the salience network, a large-scale brain system associated with homeostatic behavioral guidance [12,16]. Patients with bvFTD show early and progressive salience network dysfunction and degeneration that correlates with the characteristic social-emotional deficits of the syndrome [12]. Among all salience network nodes, the right FI has been proposed to play a central role as a major cortical hub for representing interoceptive sensory information that helps regulate autonomic tone and responses [17–20].

BvFTD is the most common syndrome within the FTD clinical spectrum and is closely linked to amyotrophic lateral sclerosis (ALS) [21,22]. Individual patients may present with bvFTD, ALS, or as a blended syndrome with elements of both (FTD with motor neuron disease, bvFTD-MND). The two disorders are also united by a shared underlying biology. Pathologically, transactive response DNA binding protein of 43 kDa (TDP-43) represents the underlying disease protein in ~50% of patients with bvFTD and nearly all with sporadic ALS [23,24]. TDP-43 is a DNA/RNA binding protein normally expressed in healthy neurons, which becomes mislocalized from the nucleus to the cytoplasm, where it aggregates into neuronal cytoplasmic inclusions [23]. FTD and ALS are usually sporadic, but they share several genetic mutations in common, the most prevalent being a hexanucleotide repeat expansion in a noncoding region of chromosome 9 open reading frame 72 (*C9orf72*) [21,22]. Importantly, patients with bvFTD who present with or develop ALS die early in their bvFTD disease course, providing an early window into pathogenesis and clinico-pathological correlations.

Recently, we completed an in-depth neuropathological study of patients who fell along the ALS/bvFTD continuum linked to TDP-43 proteinopathy. We found that early bvFTD was accompanied by selective TDP-43 aggregation within VENs and fork cells. At the level of individual neurons, TDP-43 aggregation (and accompanying loss of nuclear TDP-43) was associated with striking nuclear and somatodendritic atrophy. The proportion of neurons with TDP-43 inclusions correlated with loss of emotional empathy, as assessed by patient caregivers during life [11]. Importantly, a minority of VENs and fork cells lacked detectable nuclear TDP-43 despite the apparent absence of cytoplasmic inclusions, particularly among *C9orf72* expansion carriers. These nuclear TDP-43 depleted cells developed morphological alterations comparable to inclusion-bearing cells [11]. Although this and one previous study demonstrated that degenerating VENs and fork cells are linked to bvFTD symptoms [10,11], and neuroimaging studies suggest that social-emotional deficits are driven by salience network dysfunction [12,25,26], to date no study has evaluated the links across these levels of analysis in the same patients.

Here, we capitalized on a unique dataset that combined ante-mortem questionnaire-based assessments of emotional empathy, in vivo structural MRI, and quantitative histopathological data from 16 patients across the ALS/bvFTD clinicopathological continuum. We hypothesized that TDP-43 aggregation within VENs and fork cells would predict salience network atrophy, which, in turn, would relate to loss of empathic concern, the ability to feel and prosocially respond to others' emotions. Our findings show that VEN and fork cell inclusion formation is linked to neurodegeneration within specific insular, frontal, and subcortical sites, forming a pattern that resembles the salience network. Gray and white matter atrophy in these regions, in turn, mediates loss of emotional empathy, suggesting a chain of events linking the neuronal, brain network, and behavioral levels in producing one of the cardinal bvFTD symptoms.

Results

Over a span of ten years, 16 patients from across the ALS/bvFTD clinicopathological continuum met inclusion criteria (see Methods; Table 1). Patients were assessed with antemortem structural MRI and social-emotional function tests and postmortem neuropathological evaluation, including quantitative assessment of TDP-43 inclusion fraction and neuronal densities in right FI (see *Methods* and Figure 1). Segmented gray and white matter tissue probability maps were transformed to w-score maps (see *Methods*) [27]. Higher w-scores reflect higher voxel-wise atrophy for each patient, adjusted for demographical variables. This approach is particularly useful when performing correlational analyses with smaller samples since findings are adjusted for nuisance covariates during the preprocessing stage, preserving statistical power for the covariate of interest. Voxel-wise frequency mapping of gray matter w-scores across all patients revealed a rostral brain atrophy pattern consistent with the ALS/bvFTD clinicopathological spectrum (*SI Appendix Figure S1*). Similarly, a standardized scheme was used to assess post-mortem atrophy severity, which was mild overall (Table 1), based on coronal brain slabs [28].

TDP-43 inclusion formation in right FI VENs and fork cells correlates with gray and white matter atrophy in medial frontal, insular, limbic, and dorsomedial thalamic regions. First, we sought to explore the relationship between TDP-43 aggregation in VENs and fork cells, assessed at the cellular level, and brain atrophy, assessed across the whole brain using voxel-based morphometry. As expected, patients with pure ALS had fewer VEN and fork cell inclusions compared to patients with bvFTD and bvFTD-MND (*SI Appendix Table S1*). Voxel-wise regression analyses were used to identify gray and white matter structures in which atrophy was related to right FI VEN and fork cell inclusion fraction. Regression models were corrected for *C9orf72* mutation status and scan-to-death interval. This approach revealed that patients with a higher proportion of TDP-43 inclusions in VENs and fork cells showed more severe gray matter atrophy in frontal, insular, limbic and thalamic structures ($t = 3.9$, height threshold $p < 0.001$; cluster-extend threshold $p < 0.05$ FWE corrected); collectively, these structures included key components of the salience network. Specifically, the approach elicited the right FI, as might be expected when using a right FI-derived neuropathological predictor, as well as the pregenual anterior cingulate and paracingulate cortices, medial orbitofrontal cortex, and anterior thalamus, extending into the paraseptal area in the vicinity of the bed nucleus of the stria terminalis and spanning posteriorly the dorsomedial and medial pulvinar thalamic nuclei (Figure 2A *SI Appendix Table S2*). In the white matter analysis, we uncovered a large cluster in a region abutting the right lateral ventricle but extending into white matter proposed to connect the FI to the anterior cingulate cortex [29,30] ($t = 3.9$, height threshold $p < 0.001$; cluster-extent threshold $p < 0.05$ FWE corrected) (Figure 2B, *SI Appendix Table S2*), possibly reflecting degeneration of structural connections between these two brain regions. Importantly, to assess the influence of using w-score atrophy maps, we performed additional analyses using raw segmented gray and white matter tissue probability maps. These analyses yielded findings similar to those produced with the w-score approach, where reduced insular, frontal and subcortical gray matter was associated with higher rates of inclusion

formation in VENs and fork cells (*SI Appendix Figure S2 and Table S7*), as well as a small cluster in the amygdala, another key salience network node.

Patients with *C9orf72* expansions show extensive gray and white matter atrophy despite fewer TDP-43 inclusions in VENs and fork cells. We next plotted averaged gray and white matter atrophy from the identified clusters against VEN and fork cell inclusion formation rate, seeking to assess the distribution of *C9orf72* expansion carriers and of the three clinical syndromes (bvFTD, bvFTD-MND, ALS). Patients with ALS showed the lowest levels of atrophy and degenerating neurons, while patients with bvFTD and bvFTD-MND distributed more equally along the regression line. *C9orf72* expansion carriers showed high levels of gray matter atrophy but few inclusion-bearing neurons compared to non-expansion carriers, suggesting that factors other than TDP-43 aggregation in VENs and fork cells may contribute to network-wide gray matter atrophy in *C9orf72* expansion carriers [11,31]. Noting this possibility, we repeated the voxel-wise analyses after excluding *C9orf72* expansion carriers. These analyses revealed more widespread patterns of gray (Figure 2E, *SI Appendix Table S3*) and white matter atrophy associated with TDP-43 inclusion formation within VENs and fork cells (Figure 2F, *SI Appendix Table S3*). The identified patterns included other brain regions associated with the salience and cingulo-opercular networks, such as the left insula, right frontal operculum, and the dorsolateral prefrontal cortices ($t = 8.0$, height thresholds used $p < 0.001$ and $p < 0.0001$; cluster-extent threshold $p < 0.05$ FWE corrected)[16,32,33]. Therefore, at least in sporadic bvFTD, TDP-43 inclusion formation may impact an even broader set of brain regions.

Why do the *C9orf72* expansion carriers exhibit such a different relationship between TDP-43 aggregation and brain atrophy? The mutation is associated with several pathological features seen only in mutation carriers, including *C9orf72* haploinsufficiency, dipeptide repeat protein inclusions, and RNA foci. In addition, previous work from our group suggests that inclusion formation in VENs and fork cells is preceded by a phase of nuclear TDP-43 depletion, particularly in *C9orf72* expansion carriers, which leads to neuronal atrophy similar to TDP-43 aggregation [11]. To address whether the rate of nuclear TDP-43 depletion influences the relationship between gray matter atrophy and VEN and fork cell degeneration, we used a composite measure representing the summed rate of inclusion formation and nuclear depletion (in the absence of aggregation) in VENs and fork cells. Voxel-wise analyses corrected for *C9orf72* status and interval to death revealed limbic, thalamic, superior parietal and frontal clusters of gray matter atrophy associated with the composite measure of degenerated VENs and fork cells (*SI Appendix Figure S3 B and Table S8*) ($t = 3.9$, height threshold $p < 0.001$ cluster-extent threshold $p < 0.05$ FWE corrected). Plotting of averaged gray matter atrophy from the identified clusters against summed rates of VEN and fork cell inclusion formation and nuclear depletion resulted in *C9orf72* mutation carriers being distributed closer to the regression line when compared to the plot derived using inclusion formation rates only (Figure 2C). These findings suggest that the combination of inclusion formation and nuclear depletion may better account for frontal, limbic and thalamic atrophy, particularly among *C9orf72* expansion carriers [11].

Inclusion-bearing VENs and fork cells are associated with distinct pattern of frontal and subcortical atrophy when compared to inclusion bearing neighboring neurons in layer 5. The preceding analyses revealed patterns of gray and white matter atrophy associated with degenerating VENs and fork cells. To test the specificity of this association with these two neuronal morphotypes, we repeated the preceding analyses using the TDP-43 inclusion fraction in neighboring layer 5 neurons as the predictor. In line with previous work [11], these neighboring neurons showed lower rates of TDP-43 inclusion formation compared to VENs and fork cells, with ALS patients again having lower rates compared to patients with bvFTD-MND and bvFTD (*SI Appendix Table S1*). For this sample, the rate of inclusion bearing VENs and fork cells was highly collinear with the rate of inclusion bearing neighboring layer 5 neurons (Pearson's correlation coefficient, $R = 0.96$, $p < 0.00001$). As in the previous voxel-wise regression analyses, we corrected the models for *C9orf72* mutation status and scan-death time interval ($t = 3.9$, height threshold $p < 0.001$;

cluster-extend threshold $p < 0.05$ FWE corrected). This approach revealed partially overlapping but distinct structural correlates (Figure 2G). Similar to VENs and fork cells, in layer 5 neighboring neurons the TDP-43 aggregation rate was associated with right insular and medial thalamic gray matter atrophy ($t = 3.9$, height threshold $p < 0.001$; cluster-extent threshold $p < 0.05$ FWE corrected) (Figure 2G). In contrast to VENs and fork cells, however, layer 5 neighboring neurons lacked the association with medial frontal gray matter atrophy (Figure 2G; *SI Appendix Table S4*). Convergently, white matter atrophy was not significantly associated with inclusion formation in neighboring neurons, suggesting that VEN and fork cell degeneration may exert a specific influence on cortico-cortical fiber tracts connecting the anterior insula and cingulate/paracingulate cortices [13].

VEN and fork cell inclusion formation-linked gray and white matter atrophy correlates with deficits in empathic concern. Finally, we sought to relate the atrophy patterns associated with VEN and fork cell inclusion formation with social-emotional deficits, one of the clinical hallmarks of bvFTD [12,25]. Social-emotional function was measured using the Interpersonal Reactivity Index [34], and we focused on the empathic concern subscale because this measure best reflects the other-centered prosocial response resulting from sharing and understanding another's emotional state [25]. Moreover, previous work has linked empathic concern to the anterior insula [11,25]. Reflecting the clinical characteristics of each syndrome, in our sample empathic concern was preserved in ALS but was severely impaired in bvFTD and bvFTD-MND (*SI Appendix Table S1*). Here, we present correlation analyses between the empathic concern subscale and average atrophy levels derived from the clusters identified in the previous voxel-wise regression analyses that included all patients. First, mean gray matter atrophy values were extracted from the frontal, subcortical and right insular clusters associated with inclusion-bearing VENs and fork cells. Spearman partial correlation analyses corrected for *C9orf72* mutation status (Figure 3A), revealed that greater deficits in empathic concern were associated with more severe gray matter atrophy in frontal ($Rho = -0.86$, $p < 0.0005$), subcortical ($Rho = -0.72$, $p < 0.05$), and right insula ($Rho = -0.79$, $p < 0.005$) regions. Higher mean white matter atrophy values, derived in a like manner, also predicted greater loss of empathic concern (Figure 3B) ($Rho = -0.61$, $p < 0.05$).

The relationship between VEN and fork cell inclusion formation and loss of emotional empathy is mediated by salience network atrophy. Empathy deficits are a core feature of bvFTD and have been associated with degenerating VENs and fork cells [10–12] and with structural and functional alterations in brain regions belonging to the salience network [12,25,26]. In the present study, as in previous work, VEN and fork cell degeneration correlated with emotional empathy deficits (Pearson's correlation coefficient $R = -0.60$; $p < 0.05$). We hypothesized that salience network degeneration would mediate the link between neuron type-specific degeneration and emotional empathy deficits and tested this idea by leveraging the measures derived from this study in a structural equation model [35] (Figure 4). Structural equation models are statistical algorithms that use multiple independent regression equations to impute relationships between unobserved constructs (latent variables) from observable, measured variables. In our model, degenerating VENs and fork cells mediated salience network atrophy ($Z = 0.68$, $p < 0.001$), a latent variable composed of average gray and white matter atrophy in clusters identified in the voxel-wise analyses that included all patients. Salience network atrophy, in turn, mediated deficits in empathic concern ($Z = -0.84$, $p < 0.001$). Indices commonly used in this type of analysis to evaluate goodness of fit indicated that our model was well-suited for the observed data (*SI Appendix Table S5*). Importantly, when added to the leading model, addition of a direct path linking VEN and fork cell degeneration to emotional empathy deficits was not significant ($Z = -0.08$, $p = 0.79$), while the positive association between neuron type-specific degeneration and salience network atrophy ($Z = 0.67$, $p < 0.001$) and the negative association between salience network degeneration and empathic concern remained significant ($Z = -0.76$, $p < 0.05$). Moreover, adding a direct path linking VEN and fork cell degeneration to empathy deficits resulted in a

worse model fit, suggesting that salience network atrophy necessarily mediates the link between neuron type-specific degeneration and social-emotional deficits (*SI Appendix Figure S4 and Table S5*).

Discussion

The ALS/bvFTD clinicopathological continuum linked to TDP-43 proteinopathy provides a unique lesion model for studying the cellular and large-scale network contributors to human social-emotional functioning. Capitalizing on this opportunity, we leveraged a dataset that combined behavioral, neuroimaging, and histopathological data from the same patients with bvFTD, bvFTD-MND, and ALS. We found that selective degeneration of VENs and fork cells, as assessed by the prevalence of TDP-43 inclusions within these neurons, mediated atrophy within key salience network regions, which, in turn, mediated emotional empathy deficits in bvFTD. Notably, TDP-43 pathobiology within frontoinsular VENs and fork cells showed a neuron type-specific relationship to degeneration within anterior cingulate-paracingulate gray matter and a related white matter region; together these correlates seem positioned to connect the frontoinsular and anterior cingulate cortices. Patients with bvFTD/ALS due to the *C9orf72* repeat expansion showed a different relationship between TDP-43 inclusion formation, brain atrophy, and empathy, with substantial atrophy despite few TDP-43 inclusions in VENs and fork cells. Interestingly, patients with C9orf72 may show heightened levels of nuclear TDP-43 depletion without inclusion formation, and adding nuclear TDP-43 depleted VENs and fork cells partially recovered the relationship between VEN/fork cell TDP-43 pathobiology and brain atrophy. Overall, the findings suggest that VENs and fork cells of the frontoinsular cortex play a key role within the salience network [12,13], which, in turn, supports emotional empathy [12,25,26] likely through domain-general processes related to homeostatic behavioral guidance [12,19,20,36].

Regional correlates of VEN and fork cell degeneration: a window into connectivity? Among commonly studied laboratory mammals, VENs and fork cells are found only in the macaque monkey, and to date little information is available about the connectivity of these large, glutamatergic projection neurons [13]. Limited tract tracing studies have revealed that VENs in the macaque brain send axons to the contralateral anterior agranular insula and ipsilateral posterior/mid-insula [37]. VENs and fork cells express transcription factors associated with subcerebral projections neurons [38], suggesting the possibility of projections to autonomic control sites in the brainstem. Given the role of the salience network in viscero-autonomic processing, specific candidate VEN/fork cell projection targets include limbic/subcortical nodes of the salience network, such as the amygdala, hypothalamus, periaqueductal gray matter, and parabrachial nucleus [38].

Based on the emerging principles of network-based, transneuronal degeneration, we hypothesize that the structural correlates of VEN/fork cell inclusion formation, as revealed here, provide clues to the likely axonal connections of these cell types, a topic that can be studied only indirectly in humans. At the cortical level, VEN and fork cell inclusion formation was specifically associated with anterior cingulate/paracingulate and medial orbitofrontal degeneration, an association not found for neighboring layer 5 neurons. These regions have structural connections to the right FI [39], and in humans diffusion-weighted MRI and task-free fMRI studies have revealed structural and functional connections between these regions and FI [16,29,30,40]. A direct connection between the FI and the anterior cingulate, mediated by these cell types, would have particular functional significance. The FI has been conceived as the “afferent hub” of the salience network, equipped to build an integrated and contextualized representation of the body, including its responses to prevailing environmental conditions, while the anterior cingulate may serve as the major “efferent hub”, generating those same viscero-autonomic responses to prevailing (internal and external) conditions [36]. At the subcortical level, VEN and fork cell degeneration was specifically associated with atrophy in a cluster near the anterior thalamus, possibly extending into the bed nucleus of the stria terminalis. The bed nucleus of the stria terminalis has known projections to

salience network nodes such as the centromedial amygdala, orbitofrontal cortex, and anterior cingulate [41] and has been associated with regulating body homeostasis, stress responses, and social anxiety, facilitating reproductive behavior, and mediating social dysfunction in anxiety disorders and other psychiatric diseases [41]. Three technical limitations need to be considered when considering our findings as potential evidence of VEN/fork cell connectivity. First, our study lacked the spatial resolution to delineate subcortical areas, in particular smaller hypothalamic and brainstem nuclei involved in autonomic processing, so the absence of a relationship need not be taken to mean that VENs and fork cells do not send axons to those areas. Second, our assessment of neighboring layer 5 neurons encompassed heterogeneous neuron types, and this heterogeneity could have contributed to the differences in structural correlates observed between VENs/fork cells and other layer 5 neurons. Third, the specific connection to the anterior cingulate cortex could simply reflect the presence of VENs (and, to a much lesser degree, fork cells) in this region; patients showing greater VEN/fork cell involvement in FI may also have had greater involvement of these same vulnerable neurons in the anterior cingulate cortex, independent of spread from FI to this region.

Bridging the levels: the neural correlates of social-emotional behavior. Although feature-selective neurons exist within human sensory cortices, complex human experiences and behaviors depend on coordinated activity of distributed brain areas and their underlying neuronal circuit assemblies rather than on firing of single neurons or even neuron types [39]. Previous studies have shown that social-emotional deficits in bvFTD relate (*i*) at the neuronal level, to VEN and fork cells degeneration [10,11] and (*ii*) at the large-scale network level, to functional and structural deterioration of the salience network [12,25,26]. Our findings suggest that VEN and fork cell degeneration does not directly cause social-emotional deficits but instead leads to salience network degeneration, which, in turn, drives at least one of the core social-emotional deficits seen in bvFTD. Although very little is known about the neuronal mechanisms underlying empathy, neuroimaging studies have associated salience network integrity with social-emotional functioning in both healthy subjects [42] and clinical conditions, including sociopathy, Asperger's syndrome, and schizophrenia [33]. Among salience network nodes, the right FI has been proposed to help coordinate sympathetic outflow with highly processed sensory stimuli reflecting homeostatic, affective, motivational, and hedonic information [18,20,36,40]. The anterior and dorsomedial thalamic nuclei have known structural projections to frontal areas such as the anterior cingulate and orbitofrontal cortices [43], two regions that stood out throughout our findings. Although our results do not inform causal relationships and are derived from a relatively small sample due the laborious nature of the quantitative neuropathological methods, the novelty of this study relates to the support our data provide for a chain of influence that links specific neuronal morphotypes to brain network structure to emotional empathy, pointing towards the cellular and large-scale brain circuits that are critical for empathy. More research is needed in order to elucidate the specific role of VENs and fork cells within distinct brain regions and how they contribute to more diverse aspects of social-emotional function. We hope that the present findings will inform the anatomy of other neuropsychiatric diseases in which loss of emotional empathy is a major feature.

***C9orf72* expansion: different pathogenic mechanism or different onset neuron?** *C9orf72* repeat expansions are the most common genetic cause of FTD and ALS. In bvFTD, *C9orf72* expansion carriers exhibit social-emotional and salience network dysfunction similar to patients with sporadic disease [44–46], but carriers often show milder atrophy, which may be focally accentuated in medial thalamic nuclei [47]. Patients with *C9orf72*-bvFTD show dramatically fewer VEN and fork cell TDP-43 inclusions despite similar levels of VEN/fork cell dropout [11]. On the other hand, carriers often show higher levels of nuclear TDP-43 depletion (in the absence of inclusion formation), which is associated with neuronal degeneration comparable to that seen in TDP-43 inclusion-bearing neurons [11]. Our findings show that *C9orf72* expansion carriers have higher than expected gray matter atrophy given their low rates of TDP-43 inclusion formation compared to non-carriers. The relationship between TDP-43 pathobiology and regional atrophy

was stronger when using a combined measure of TDP-43 inclusion formation and nuclear depletion in VENs and fork cells, suggesting that nuclear depletion or dysfunction may trigger processes leading to salience network degeneration [31] or that VENs and fork cells are affected due to a non-TDP-43 mechanism such as RNA aggregation or dipeptide repeat protein toxicity. Alternatively, VENs and fork cells may not be the initial onset neurons in *C9orf72*-related bvFTD, which may begin in different neuronal populations or within other nodes of the salience network, such as the medial pulvinar nucleus of the thalamus [31].

Methods

Subjects. Patients were selected from a previous histopathological study [11] based on availability of a complete neuroimaging and histopathological dataset (Table 1). Patients were required to have (*i*) a clinical diagnosis of bvFTD, bvFTD-MND, or ALS, *(ii*) a neuropathological diagnosis of (1) frontotemporal lobar degeneration with TDP-43 pathology (FTLD-TDP), Types B or unclassifiable, (with or without MND) or (2) ALS-TDP. We focused on FTLD-TDP Types B and unclassifiable since these are the most common forms seen in patients along the ALS/bvFTD continuum [21,22]. Focusing on a single clinical and neuropathological continuum allowed us to access variation in empathy deficits, brain network atrophy patterns, and neuron type-specific degeneration among patients. Seven patients were *C9orf72* mutation positive. Patients known to carry disease-causing mutations other than *C9orf72* repeat expansions were excluded. Based on these criteria, we included 16 patients in total (Table 1): five patients with bvFTD, nine with bvFTD-MND, and two with ALS.

Neuropsychological and emotional empathy assessment. A multidisciplinary team determined patients' clinical diagnoses following thorough neurological, neuroimaging and neuropsychological assessments. Clinical severity was assessed using the Mini Mental State Examination (MMSE) and the Clinical Dementia Rating (CDR) scale total and sum of boxes scores, using a version of the CDR adapted for FTD [48]. In 13 out of 16 patients, the empathic concern subscale of the Interpersonal Reactivity Index [34] was completed by the patient's informant. The empathic concern subscale measures emotional aspects of empathy, in particular the other-centered emotional response resulting from the perception of another's emotional state. It consist of 7 questions that can comprehensively reach a maximum score of 28. All neuropsychological assessments were obtained within 90 days of structural neuroimaging.

Structural Neuroimaging. Details regarding acquisition and preprocessing of structural and functional images are provided in the *SI Appendix, Supplementary Experimental Procedures*. Briefly, structural MRI images were acquired at UCSF or at the San Francisco Veterans Affairs Medical Center (SFVAMC) and underwent a voxel-based morphometry analysis [49] after being visually inspected for motion and scanning artifacts. Structural images were segmented in gray matter, white matter, and cerebrospinal fluid and normalized to MNI space using SPM12 (http://www.fil.ion.ucl.ac.uk/spm/software/spm12/). Gray and white matter images were modulated by dividing the tissue probability values by the Jacobian of the warp field, and smoothed with an isotropic Gaussian kernel with a full width at half maximum of 8 mm. The smoothed images were finally transformed to w-score maps [27]. W-scores are analogous to z-scores adjusted for specific covariates [50,51]. Higher w-scores reflect higher levels of atrophy for the specific subject after adjustment. For this study, covariates included age, sex, education, handedness, scanner type, and total intracranial volume. W-score maps were derived using a sample of 288 healthy older adults (*SI Appendix Table S6*), where voxel-wise regressions were first performed to model the relationship between the covariates and neuroimaging data in this sample. Subsequently, w-score maps were computed as follows:

$$W = \frac{(Raw - Expected)}{SD\varepsilon}$$

Where *Raw* is the raw value of a voxel from the smoothed image of a patient; *Expected* is the expected value for the voxel of that specific patient based on the healthy control model; and *SDε* is the standard deviation of the residuals from the healthy control model.

Histopathology. Patients died 2.4 +/- 1.9 years after neuroimaging acquisition. Details on specimen and tissue processing can be found in previous work [11] and in *SI Appendix, Supplementary Experimental Procedures*. The present neuropathological data represent a subset of the data reported previously [11] and no new neuropathological data were collected for the present study. Briefly, postmortem research-oriented autopsies were performed at the UCSF Neurodegenerative Disease Brain Bank. Consent for brain donation was obtained from all subjects or their surrogates in accordance with the Declaration of Helsinki. Neuropathological diagnoses were made following consensus diagnostic criteria [24,52–55] based on histological and immunohistochemical methods [10,56]. Anatomical disease stage was assessed by a single blinded investigator (W.W.S) using an FTD rating scale [28]. Blocks of the right FI were dissected, sectioned at 50 microns, and Nissl-stained to determine layer 5 within the anatomical boundaries of the right FI. Sections were stained for TDP-43 using an antibody that recognizes both full-length normal and pathological forms of the protein. Again in layer 5 of the right FI, unbiased counting on microscope-derived images was used to obtain the proportion of each cell type (VENs, fork cells, and neighboring neurons) characterized by normal TDP-43, a cytoplasmic inclusion, or nuclear TDP-43 depletion.

Statistical analyses. In SPM 12, voxel-wise regression analyses were separately performed on gray and white matter w-score maps using the rate of inclusion-bearing VENs and fork cells of the right FI as the independent variable. Models were corrected for *C9orf72* mutation status and time interval between scanning and death. We further assessed the impact of right FI VEN and fork cell densities by modelling densities as covariate of no interest using a quadratic polynomial function in our voxel-wise control analyses. A height threshold of $p < 0.001$ and a cluster-extend threshold of $p < 0.05$ FWE corrected was used in all voxel-wise analyses if not reported otherwise. To explore differences between *C9orf72* mutation positive and negative patients, average levels of atrophy in the identified brain clusters were plotted against the rate of TDP-43 inclusion bearing VENs and fork cells using Matlab (https://www.mathworks.com/products/matlab.html). Control analyses were carried out by excluding patients with *C9orf72* mutations from voxel-wise regression models. To further explore the relationship between cellular degeneration and *C9orf72* status, voxel-wise regression analyses were performed on gray matter w-score maps using the summed rate of TDP-43 inclusion-bearing and depleted VENs and fork cells of the right FI as the independent variable. To explore the neuron type-specific associations of atrophy patterns with neurodegeneration of VENs and fork cells, similar voxel-wise regression analyses were performed using the rate of inclusion bearing neighboring neurons in layer 5 of the right FI as the independent variable. Average levels of regional gray and white matter atrophy associated with inclusion bearing VENs and fork cells were associated with the empathic concern score of the Interpersonal Reactivity Index using Spearman partial correlation corrected for *C9orf72* mutation status ($p < 0.05$). Finally, a structural equation model was conducted in R (https://www.r-project.org/; *SI Appendix, Supplementary Experimental Procedures*) to test whether brain network-based gray and white matter atrophy mediates the link between neuron type-specific degeneration and empathy deficits in FTD.

Acknowledgements

This study was supported by NIH grants R01AG033017 (WWS), K08 AG052648 (SS), P01AG019724 and P50AG023501 (BLM), and the John Douglas French Alzheimer's Foundation (GC). LL was supported by the Reserve Talents of Universities Overseas Research Program of Heilongjiang in China (Document Number:

Heijiaogao [2012]381). We thank the patients and their families for their invaluable contributions to FTD/MND research.

Conflict of interests

The authors of this study declare the absence of competing conflict of interests.

References

1. Seeley, W. Mapping Neurodegenerative Disease Onset and Progression. *Cold Spring Harb. Perspect. Biol.* **1389**, (2017).

2. Brettschneider, J., Del Tredici, K., Lee, V. M.-Y. & Trojanowski, J. Q. Spreading of pathology in neurodegenerative diseases: a focus on human studies. *Nat. Rev. Neurosci.* **16**, 109–20 (2015).

3. Seeley, W. W., Crawford, R. K., Zhou, J., Miller, B. L. & Greicius, M. D. Neurodegenerative Diseases Target Large-Scale Human Brain Networks. *Neuron* **62**, 42–52 (2009).

4. Fu, H., Hardy, J. & Duff, K. E. Selective vulnerability in neurodegenerative diseases. *Nat. Neurosci.* **21**, 1350–1358 (2018).

5. Braak, H. & Braak, E. Neuropathological stageing of Alzheimer-related changes. *Acta Neuropathol.* **82**, 239–59 (1991).

6. Braak, H., Braak, E. & Bohl, J. Staging of Alzheimer-Related Cortical Destruction. *Eur. Neurol.* **33**, 403–408 (1993).

7. Grinberg, L. T. *et al.* The dorsal raphe nucleus shows phospho-tau neurofibrillary changes before the transentorhinal region in Alzheimer's disease. A precocious onset? *Neuropathol. Appl. Neurobiol.* **35**, 406–416 (2009).

8. Ossenkoppele, R. *et al.* Tau PET patterns mirror clinical and neuroanatomical variability in Alzheimer's disease. *Brain* **139**, 1551–1567 (2016).

9. Zhou, J., Gennatas, E. D., Kramer, J. H., Miller, B. L. & Seeley, W. W. Predicting Regional Neurodegeneration from the Healthy Brain Functional Connectome. *Neuron* **73**, 1216–1227 (2012).

10. Kim, E. J. *et al.* Selective frontoinsular von economo neuron and fork cell loss in early behavioral variant frontotemporal dementia. *Cereb. Cortex* **22**, 251–259 (2012).

11. Nana, A. L. *et al.* Neurons selectively targeted in frontotemporal dementia reveal early stage TDP-43 pathobiology. *Acta Neuropathol.* **137**, 27–46 (2018).

12. Seeley, W. W., Zhou, J. & Kim, E.-J. Frontotemporal Dementia: What Can the Behavioral Variant Teach Us about Human Brain Organization? *Neurosci.* **18**, 373–385 (2012).

13. Allman, J. M. *et al.* The von Economo neurons in the frontoinsular and anterior cingulate cortex. *Ann. N. Y. Acad. Sci.* **1225**, 59–71 (2011).

14. Stimpson, C. D. *et al.* Biochemical specificity of von economo neurons in hominoids. *Am. J. Hum. Biol.* **23**, 22–28 (2011).

15. Nimchinsky, E. A., Vogt, B. A., Morrison, J. H. & Hof, P. R. Spindle neurons of the human anterior cingul. Ate cortex. *J. Comp. Neurol.* **355**, 27–37 (1995).

16. Seeley, W. W. *et al.* Dissociable intrinsic connectivity networks for salience processing and executive control. *J Neurosci* **27**, 2349–2356 (2007).

17. Craig, A. D. Forebrain emotional asymmetry: A neuroanatomical basis? *Trends Cogn. Sci.* **9**, 566–571 (2005).

18. (Bud) Craig, A. D. How do you feel — now? The anterior insula and human awareness. *Nat. Rev. Neurosci.* **10**, 59–70 (2009).

19. Sturm, V. E. *et al.* Network architecture underlying basal autonomic outflow: Evidence from frontotemporal dementia. *J. Neurosci.* 0347–18 (2018). doi:10.1523/JNEUROSCI.0347-18.2018

20. Critchley, H. D. & Harrison, N. A. Visceral Influences on Brain and Behavior. *Neuron* **77**, 624–638 (2013).

21. DeJesus-Hernandez, M. *et al.* Expanded GGGGCC Hexanucleotide Repeat in Noncoding Region of C9ORF72 Causes Chromosome 9p-Linked FTD and ALS. *Neuron* **72**, 245–256 (2011).

22. Renton, A. E. *et al.* A Hexanucleotide Repeat Expansion in C9ORF72 Is the Cause of Chromosome 9p21-Linked ALS-FTD. *Neuron* **72**, 257–268 (2011).

23. Neumann, M. *et al.* Ubiquitinated TDP-43 in Frontotemporal Lobar Degeneration and Amyotrophic Lateral Sclerosis. *Science (80-.).* **314**, 130–133 (2006).

24. MacKenzie, I. R. A. *et al.* Nomenclature and nosology for neuropathologic subtypes of frontotemporal lobar degeneration: An update. *Acta Neuropathol.* **119**, 1–4 (2010).

25. Rankin, K. P. *et al.* Structural anatomy of empathy in neurodegenerative disease. *Brain* **129**, 2945–2956 (2006).

26. Toller, G. *et al.* Individual differences in socioemotional sensitivity are an index of salience network function. *Cortex* 1–13 (2018). doi:10.1016/j.cortex.2018.02.012

27. La Joie, R. *et al.* Region-Specific Hierarchy between Atrophy, Hypometabolism, and -Amyloid (A) Load in Alzheimer's Disease Dementia. *J. Neurosci.* **32**, 16265–16273 (2012).

28. Broe, M. *et al.* Staging disease severity in pathologically confirmed cases of frontotemporal dementia. *Neurology* **60**, 1005–1011 (2003).

29. Ghaziri, J. *et al.* The Corticocortical Structural Connectivity of the Human Insula. *Cereb. Cortex* **27**, 1216–1228 (2017).

30. Cerliani, L. *et al.* Probabilistic tractography recovers a rostrocaudal trajectory of connectivity variability in the human insular cortex. *Hum. Brain Mapp.* **33**, 2005–2034 (2012).

31. Vatsavayai, S. C. *et al.* Timing and significance of pathological features in *C9orf72* expansion-associated frontotemporal dementia. *Brain* aww250 (2016). doi:10.1093/brain/aww250

32. Touroutoglou, A., Hollenbeck, M., Dickerson, B. C. & Feldman Barrett, L. Dissociable large-scale networks anchored in the right anterior insula subserve affective experience and attention. *Neuroimage* **60**, 1947–1958 (2012).

33. Menon, V. & Uddin, L. Q. Saliency, switching, attention and control: a network model of insula function. *Brain Struct. Funct.* 1–13 (2010). doi:10.1007/s00429-010-0262-0

34. Davis, M. H. A. A Multidimensional Approach to Individual Differences in Empathy. (2007).

35. Kline, R. B. *Principles and practice of structural equation modeling*.

36. Zhou, J. & Seeley, W. W. Network Dysfunction in Alzheimer ' s Disease and Frontotemporal Dementia : Implications for Psychiatry. *Biol. Psychiatry* **75**, 565–573 (2014).

37. Evrard, H. C., Forro, T. & Logothetis, N. K. Von Economo Neurons in the Anterior Insula of the Macaque Monkey. *Neuron* **74**, 482–489 (2012).

38. Cobos, I. & Seeley, W. W. Human von economo neurons express transcription factors associated with Layer v subcerebral projection neurons. *Cereb. Cortex* **25**, 213–220 (2015).

39. Mesulam, M.-M. Large-scale neurocognitive networks and distributed processing for attention, language, and memory. *Ann. Neurol.* **28**, 597–613 (1990).

40. Uddin, L. Q. Salience processing and insular cortical function and dysfunction. *Nat. Rev. Neurosci.* **16**, 55–61 (2014).

41. Lebow, M. A. & Chen, A. Overshadowed by the amygdala : the bed nucleus of the stria terminalis emerges as key to psychiatric disorders. **21**, 450–463 (2016).

42. Shamay-Tsoory, S. G. The Neural Bases for Empathy. *Neurosci.* **17**, 18–24 (2011).

43. Pergola, G. *et al.* The Regulatory Role of the Human Mediodorsal Thalamus. *Trends Cogn. Sci.* **22**, 1011–1025 (2018).

44. Boxer, A. L. *et al.* Clinical, neuroimaging and neuropathological features of a new chromosome 9p-linked FTD-ALS family. *J. Neurol. Neurosurg. Psychiatry* **82**, 196–203 (2011).

45. Sha, S. J. *et al.* Frontotemporal dementia due to C9ORF72 mutations: Clinical and imaging features. *Neurology* **79**, 1002–1011 (2012).

46. Irwin, D. J. *et al.* Cognitive decline and reduced survival in *C9orf72* expansion frontotemporal degeneration and amyotrophic lateral sclerosis. *J. Neurol. Neurosurg. Psychiatry* **84**, 163–169 (2013).

47. Lee, S. E. *et al.* Altered network connectivity in frontotemporal dementia with C9orf72 hexanucleotide repeat expansion. *Brain* **137**, 3047–3060 (2014).

48. Knopman, D. S. *et al.* Development of methodology for conducting clinical trials in frontotemporal lobar degeneration. *Brain* **131**, 2957–68 (2008).

49. Ashburner, J. & Friston, K. J. Voxel-based morphometry - The methods. *Neuroimage* **11**, 805–821 (2000).

50. Boccardi, M. *et al.* The MRI pattern of frontal and temporal brain atrophy in fronto-temporal dementia. *Neurobiol. Aging* **24**, 95–103 (2003).

51. Jack, C. R. *et al.* Medial temporal atrophy on MRI in normal aging and very mild Alzheimer's disease. *Neurology* **49**, 786–94 (1997).

52. Mackenzie, I. R. A. & Neumann, M. Molecular neuropathology of frontotemporal dementia: insights into disease mechanisms from postmortem studies. *J. Neurochem.* **138**, 54–70 (2016).

53. McKeith, I. G. *et al.* Diagnosis and management of dementia with Lewy bodies: Third report of the DLB consortium. *Neurology* **65**, 1863–1872 (2005).

54. McKeith, I. G. *et al.* Diagnosis and management of dementia with Lewy bodies. *Neurology* **89**, 88–100 (2017).

55. Montine, T. J. *et al.* National Institute on Aging-Alzheimer's Association guidelines for the neuropathologic assessment of Alzheimer's disease: a practical approach. *Acta Neuropathol.* **123**, 1–11 (2012).

56. Tartaglia, M. C. *et al.* Sporadic corticobasal syndrome due to FTLD-TDP. *Acta Neuropathol.* **119**, 365–74 (2010).

Figure legends

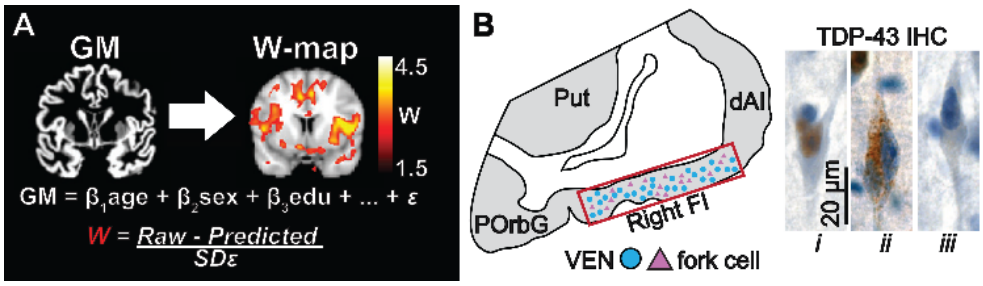

Figure 1. Patient assessment. (A) All patients underwent structural MRI. Images were preprocessed, segmented into gray and white matter tissue intensity maps, and transformed to w-score maps using a multiple regression model in healthy older adults to model the voxel-wise relationship between relevant demographic variables and segmented tissue intensity. The model provides a predicted gray matter map for each patient, and the actual and predicted gray matter maps are compared to derive w-score maps, which reflect the deviation at each voxel from the predicted gray or white matter intensity. Higher w-scores reflect more atrophy. (B) Post-mortem, the rate of TDP-43 depleted and inclusion bearing VENs (blue circles) and fork cells (violet triangles) was quantified in Layer 5 of the right FI via unbiased counting on TDP-43 immunostained sections. TDP-43 is normally expressed in the nucleus (*i*, brown nucleus in normal fork cell to left), which in patients aggregates into neuronal cytoplasmic inclusions (*ii*, middle VEN) while being cleared from the nucleus. A minority of neurons lacks either normal nuclear TDP-43 or a cytoplasmic inclusion (*iii*, nuclear TDP-43 depleted VEN). Panel B adapted with permission from reference 11. dAI = dorsal anterior insula; FI = frontoinsular cortex; IHC = immunohistochemistry; GM = gray matter; POrbG = posterior orbitofrontal gyrus; *Predicted* = through the healthy adults regression model predicted patient's gray matter map; Put = putamen ; *Raw* = segmented patient's gray matter map; *SDε* = standard deviation of the residuals in the healthy adults model; TDP-43 = transactive response DNA binding protein with 43 kD; VEN = von Economo neuron.

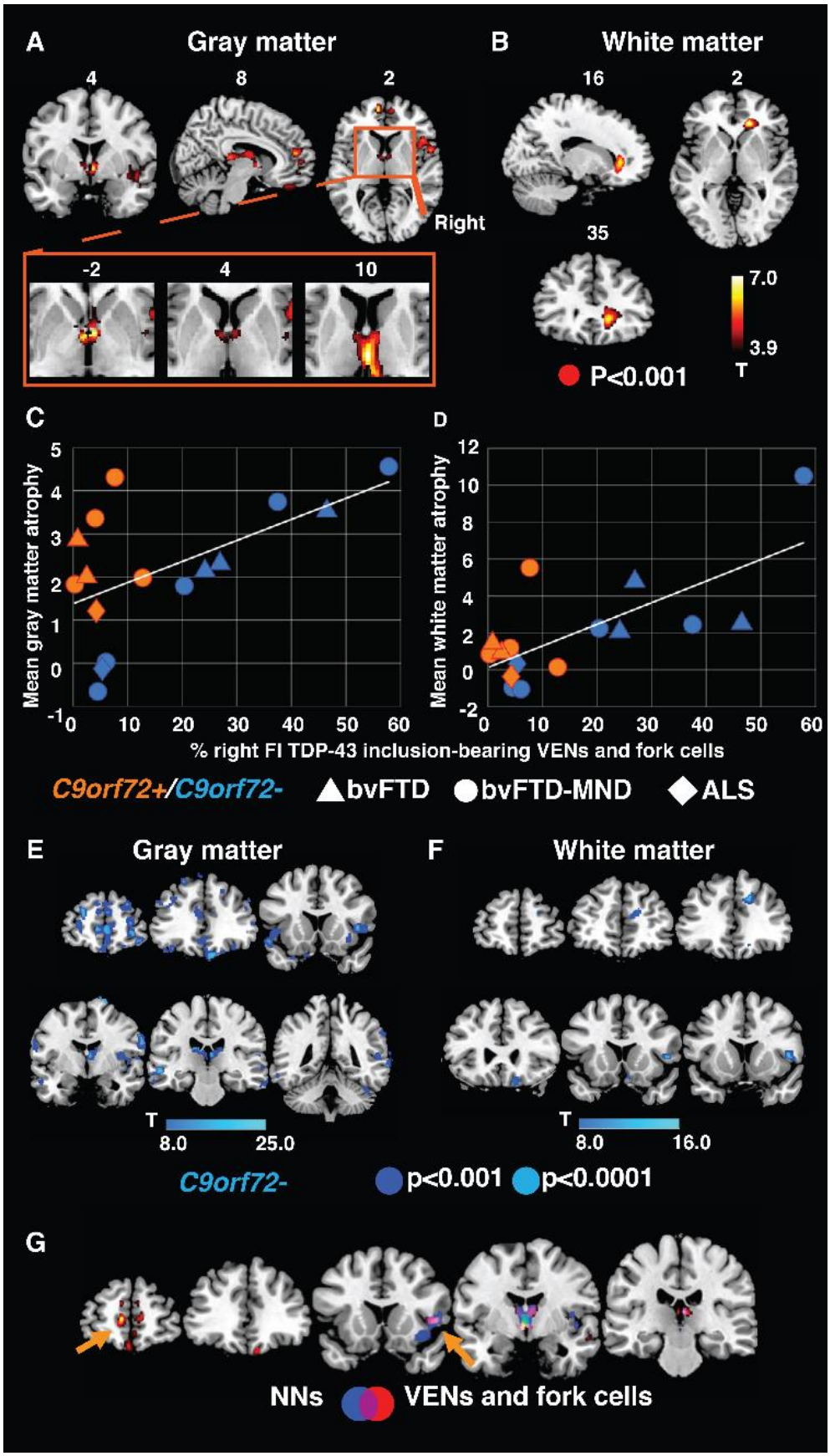
A
Gray matter
4
8
2
Right
-2
4
10
B
White matter
16
2
35
7.0
3.9
T
P<0.001
C
Mean gray matter atrophy
% right FI TDP-43 inclusion-bearing VENs and fork cells
D
Mean white matter atrophy
C9orf72+/C9orf72-
bvFTD
bvFTD-MND
ALS
E
Gray matter
T
8.0
25.0
F
White matter
T
8.0
16.0
C9orf72-
p<0.001
p<0.0001
G
NNs
VENs and fork cells

Figure 2. Gray and white matter atrophy associated with the rate of TDP-43 inclusion-bearing VENs and fork cells in right FI (A) Associated gray matter atrophy was observed in medial frontal, right insular, subcortical, limbic, and dorsomedial thalamic sites. A cluster in anterior limbic areas is seen in the region of the bed nucleus of the stria terminalis, and subcortical areas span posteriorly into the dorsomedial and medial pulvinar thalamic nuclei. (B) Associated white matter atrophy consisted of a cluster in proximity to the anterior cingulate cortex and right anterior insula. In (A) and (B), voxel-wise analyses were corrected for *C9orf72* mutation status and the interval between MRI scan and death. Averaged levels of gray matter (C) and white matter (D) atrophy in the identified clusters plotted against the rate of TDP-43 inclusion-bearing VENs and fork cells. Notably, *C9orf72* expansion carriers (orange) showed high levels of gray matter atrophy despite a low proportion of inclusion-bearing neurons compared to non-expansion carriers (blue). Control analyses without *C9orf72* expansion carriers revealed more widespread patterns of gray matter (E) and white matter (F) atrophy associated with TDP-43 inclusion-bearing VENs and fork cells. Voxel-wise analyses were performed with a height threshold of $p < 0.001$ if not specified otherwise; and a cluster-extent threshold of $p < 0.05$ FWE, corrected. ALS = amyotrophic lateral sclerosis (diamonds); bvFTD = behavioral variant frontotemporal dementia (triangles); *C9orf72* = chromosome 9 open reading frame 72 expansion carriers; bvFTD-MND = bvFTD with motor neuron disease (circles).

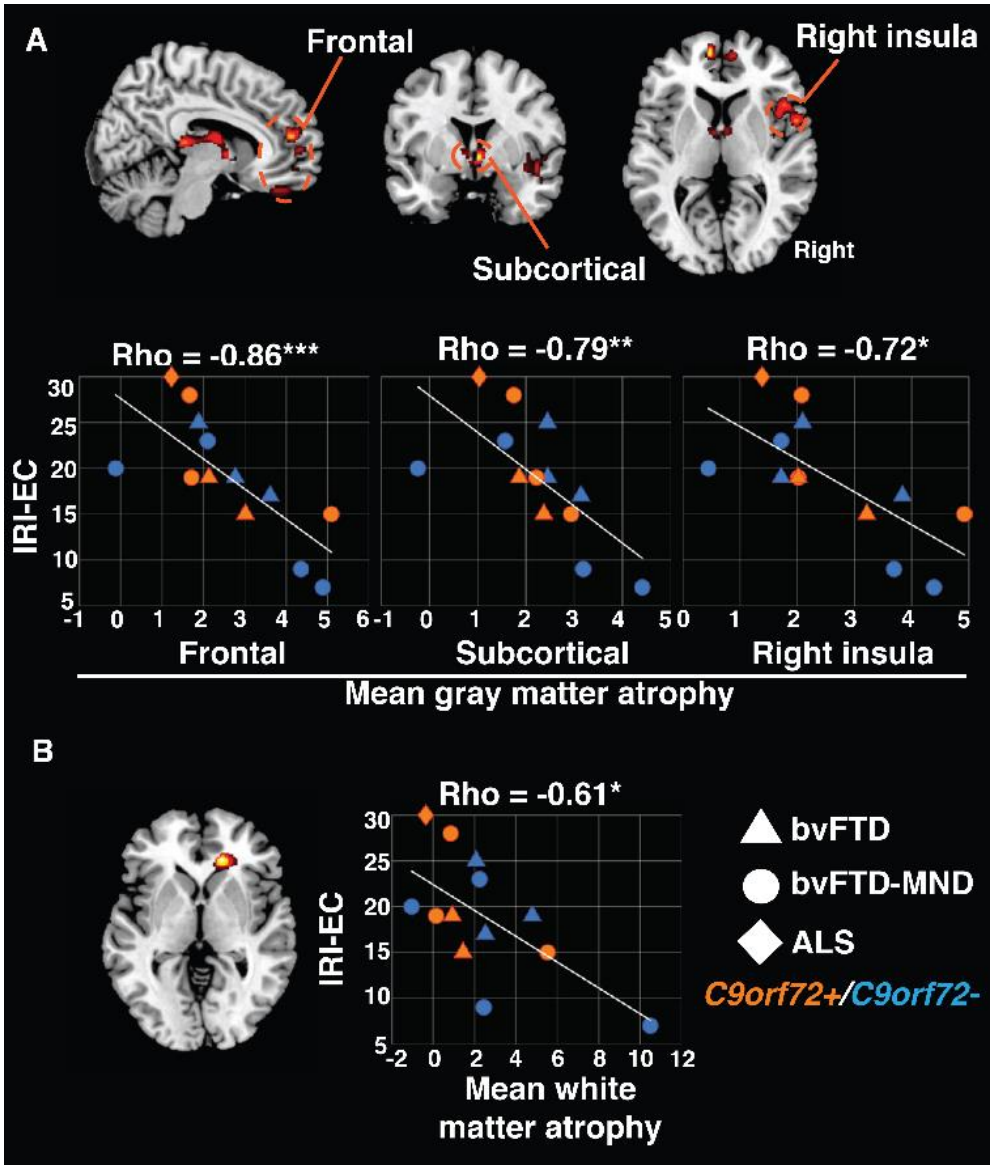

Figure 3. Loss of emotional empathy is associated with atrophy in regions related to VEN and fork cell inclusion formation. (A) Frontal, subcortical, and right insula gray matter atrophy associated with degenerating VENs and fork cells each correlate with deficits in empathic concern. (B) White matter atrophy associated with inclusion formation in VENs and fork cells shows a similar relationship. Spearman partial correlation Rho; corrected for *C9orf72* mutation status; $p < 0.05$. IRI-EC = Interpersonal Reactivity Index, empathic concern subscale.

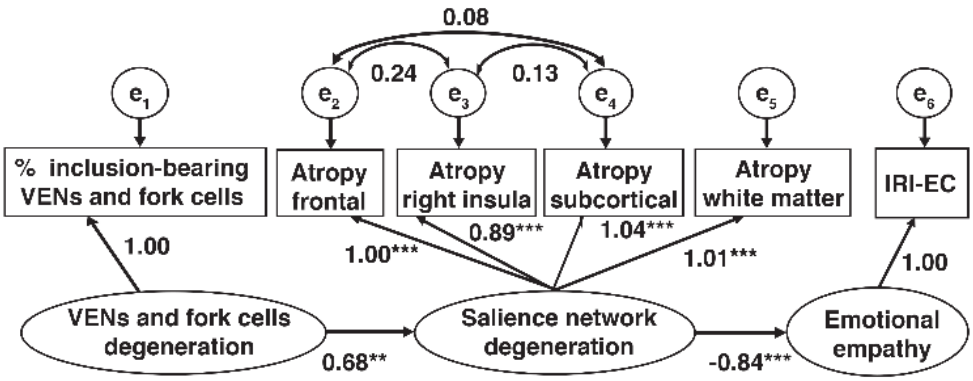

Figure 4. Structural equation model for representing the relationships between neuron type-specific degeneration, regional brain atrophy, and loss of emotional empathy. The output of a structural equation model is a diagram, where latent variables are shown as ovals, observed variables as rectangles, and standardized coefficients for each of the parameters (arrows) in the model indicate the strength of the relationships between variables. Error terms are usually estimated to model the unreliability of measures on parameter estimation and to improve the model. In the model, degenerating VENs and fork cells mediated salience network gray and white matter degeneration, which, in turn, mediated emotional empathy deficits in bvFTD. The unreliability of measures on parameter estimation is modeled through error terms (e). **$p < 0.001$; ***$p < 0.0001$

Table 1. Demographics and sample characteristics

N	16
Clinical diagnoses	2 ALS; 9 bvFTD-MND; 5 bvFTD
Pathological diagnoses	4 FTLD-TDP-B; 1 FTLD-TDP-U; 6 FTLD-TDP-B, MND; 2 FTLD-TDP-U, MND; 3 ALS-TDP
C9orf72 expansion carriers *(-:+)*	7:9
Gender (Female:Male)	10:6
Age at MRI scan in years	60.1 (6.3)
Scan-death interval in years	2.4 (1.9)
Handedness (Left:Ambidextrous:Right)	0:0:16
Education in years	15.9 (2.8)
Total intracranial volume in liters	1.5 (0.2)
Broe stage, median (range)	1 (0-2)
% of TDP-43 inclusion bearing VENs and fork cells	16.3 (17.7)
% of TDP-43 inclusion bearing NNs	5.3 (6.2)
CDR Total	1.6 (1.3)
CDR Sum Of Boxes	7.1 (5.0)
MMSE	23.4 (7.8)
IRI, empathic concern subscale (N = 13)	18.9 (6.7)

Unless otherwise noted, numbers in parentheses are SD of preceding mean. CDR = Clinical Dementia Rating. IRI = Interpersonal Reactivity Index, the empathic concern subscale can reach a maximal attainable score of 28. MMSE = Mini Mental State Examination.